Modeling Three-Dimensional Discontinuities in Waveguides Using Nonorthogonal FDTD Algorithm

Jin-Fa Lee, *Member, IEEE,* Robert Palandech, and Raj Mittra, *Fellow, IEEE*

Abstract—**In this paper, we present a generalization of the finite difference time domain (FDTD) algorithm adapted to nonorthogonal computational grids and apply it to the investigation of three dimensional discontinuity problems. The nonorthogonal FDTD uses a body-fitted grid for meshing up the computation domain and, consequently, is able to model the problem geometry with better accuracy than is possible with the staircasing approach conventionally employed in the FDTD algorithm. In addition to extending the FDTD algorithm to nonorthogonal grids, we also derive the stability conditions for the nonorthogonal FDTD algorithm in two and three dimensions. Numerical results including an *H*-plane waveguide junction, a circular waveguide with a circular iris, a circular waveguide with a rectangular iris, and a microstrip bend discontinuity, are presented to validate the current nonorthogonal FDTD approach.**

I. Introduction

THE MICROWAVE discontinuity problems in three dimensions often involve complicated shapes. In using the conventional FDTD algorithm [1] to model such problems, a staircased mesh is often employed. This approach suffers from the disadvantage that an accurate description of a non-Cartesian geometry usually requires a very fine mesh and, consequently, a very small time step in the FDTD algorithm.

To circumvent this problem, Holland [2] has generalized the FDTD algorithm to general nonorthogonal grids. Using the nonorthogonal FDTD mesh enables one to conform to the shape of a three-dimensional structure and, therefore, avoid the problem of a very small time step resulting from an overly dense mesh. In this paper, we first modify Holland's formulation in order to improve its computational efficiency, and then apply it to study some three-dimensional discontinuity problems. Additionally, we perform the stability analysis of the nonorthogonal FDTD algorithm in two and three dimensions, and derive an upper bound for the time step that guarantees stable numerical solutions. The study of several microwave junctions, viz., an *H*-plane waveguide discontinuity, a circular waveguide with a circular iris, a circular waveguide with a rectangular iris, and a microstrip bend discontinuity, are presented to validate the current approach.

This paper is organized as follows. Section II presents the formulation which extends the FDTD algorithm to nonorthogonal grids. The corresponding stability analyses for two- and three-dimensional geometries are presented in Section III. Several numerical results are included in Section IV, and brief conclusions are given in Section V.

Manuscript received April 9, 1991; revised August 1, 1991.

J.-F. Lee was with the Electromagnetic Communication Laboratory, Department of Electrical and Computer Engineering, University of Illinois 1406 N. Green St., Urbana, IL 61801-2991. He is presently with the Department of Electrical Engineering, Worcester Polytechic Institute, Worcester, MA 01609.

R. Palandech was with the Department of Electrical and Computer Engineering, University of Illinois, 1406 W. Green St., Urbana, IL 61801-2991. He is presently with Motorola, Inc., 1301 E. Algonquin Rd., Schaumburg, IL 60196.

R. Mittra is with the Electromagnetic Communication Laboratory, Department of Electrical and Computer Engineering, University of Illinois, 1406 W. Green St., Urbana, IL 61801-2991.

IEEE Log Number 9105249.

II. Three-Dimensional Nonorthogonal FDTD Algorithm

The formulation of the FDTD algorithm in nonorthogonal computational grids has been presented by Holland [2] and, in [3], Fusco has successfully used this approach to solve two-dimensional scattering problems. In this paper, we reformulate the nonorthogonal FDTD algorithm using the covariant and contravariant components of the electric and magnetic fields as the unknown variables. This modification results in a more efficient time marching procedure than that presented in [2].

A nonorthogonal coordinate system (u^1, u^2, u^3) in three dimensions may be characterized [4] by a set of vectors $\boldsymbol{A}_i$ (see Fig. 1) where

$$d\vec{r} = \sum_{i=1}^{3} \frac{\partial \vec{r}}{\partial u^i} du^i = \sum_{i=1}^{3} \boldsymbol{A}_i du^i \tag{1}$$

From Fig. 1, we see that the bases $\boldsymbol{A}_i$ are vectors defined by the edges of the cell. According to Fig. 1, we can also define a dual bases (reciprocal bases) $\boldsymbol{A}^i$ as follows

$$\boldsymbol{A}^1 = \frac{\boldsymbol{A}_2 \times \boldsymbol{A}_3}{\sqrt{g}}$$
$$\boldsymbol{A}^2 = \frac{\boldsymbol{A}_3 \times \boldsymbol{A}_1}{\sqrt{g}}$$
$$\boldsymbol{A}^3 = \frac{\boldsymbol{A}_1 \times \boldsymbol{A}_2}{\sqrt{g}} \tag{2}$$

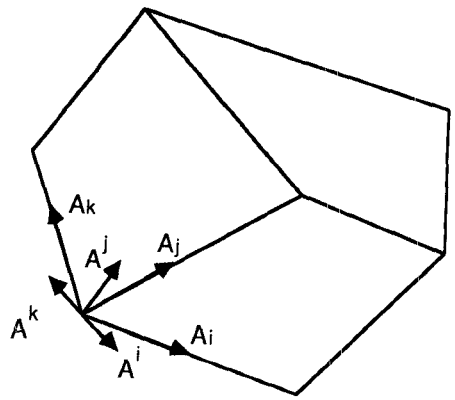

Fig. 1. Reciprocal basis vectors for the nonorthogonal coordinate system.

where $\sqrt{g}$ is the volume enclosed by the unit cell. A dual basis vector, say A_i, points in the direction normal to the face i, which is a quadrilateral area spanned by A_j and A_k (i, j, k are cyclical indices). Furthermore, the dual bases A^i's and the original bases A_i's satisfy the reciprocal relationship:

$$A^i \cdot A_j = \delta_{ij} \tag{3}$$

where δ_{ij} is the usual Kronecker delta. An arbitrary vector can be written in two-forms expressed by these two bases. For example, the electric field $\vec{E}$, can be expressed in terms of these two bases as

$$\vec{E} = \sum_i E^i A_i$$

$$\vec{E} = \sum_i A^i E_i \tag{4}$$

Here, the coefficients E^i and E_i are called the contravariant and covariant components [4], respectively, of the electric field $\vec{E}$.

The physical meanings of the covariant and contravariant components will now be given. We first use the second equation in (4) to find the *flow* of the electric field along the edge i, i.e., $\vec{E} \cdot A_i$. From the reciprocal relationship in (3), we obtain

$$\vec{E} \cdot A_i = \left(\sum_j A^j E_j \right) \cdot A_i = E_i \tag{5}$$

We therefore conclude from (5) that the covariant component E_i represents the *flow* of $\vec{E}$ along the edge i. Similarly, by taking the inner product of the first equation in (4) with the dual basis A^i, and using the reciprocal relationship in (3), we get

$$\vec{E} \cdot A^i = \left(\sum_j E^j A_j \right) \cdot A^i = E^i \tag{6}$$

From (2) and (6), the contravariant component E^i is seen to be the total flux of the electric field passing through face i, divided by the volume $\sqrt{g}$.

To extend the FDTD algorithm to nonorthogonal grids, we need to approximate Maxwell's equations in terms of the contravariant and covariant components. To this end, we start from the source-free, integral form of Maxwell's equations, for isotropic media, given below:

$$-\frac{\partial}{\partial t} \int_\Omega \mu \vec{H} \cdot d\boldsymbol{a} = \oint_{\partial\Omega} \vec{E} \cdot d\boldsymbol{l}$$

$$\frac{\partial}{\partial t} \int_\Omega \epsilon \vec{E} \cdot d\boldsymbol{a} = \oint_{\partial\Omega} \vec{H} \cdot d\boldsymbol{l} \tag{7}$$

The left hand sides of (7) represent the time rates of change of the electric and the magnetic flux through a surface Ω, whereas the right hand sides of (7) give the *circulations* of the electric and magnetic fields along the corresponding closed boundary $\partial\Omega$. From above, we can obtain a finite difference approximation of the Faraday's law:

$$\begin{aligned} E^1(I, J, K)^{n+1} &= E^1(I, J, K)^n + \frac{\Delta t}{\epsilon \sqrt{g}} \left[H_3\left(I, J + \frac{1}{2}, K\right) \right. \\ &\quad - H_3\left(I, J - \frac{1}{2}, K\right) - H_2\left(I, J, K + \frac{1}{2}\right) \\ &\quad \left. + H_2\left(I, J, K - \frac{1}{2}\right) \right]^{n+1/2} \end{aligned} \tag{8}$$

The other two components, E^2 and E^3, can be derived simply by index permutations. Likewise, the finite difference forms of the Ampere's law read

$$\begin{aligned} H^1(I, J, K)^{n+1/2} &= H^1(I, J, K)^{n-1/2} - \frac{\Delta t}{\mu \sqrt{g}} \left[E_3\left(I, J + \frac{1}{2}, K\right) \right. \\ &\quad - E_3\left(I, J - \frac{1}{2}, K\right) - E_2\left(I, J, K + \frac{1}{2}\right) \\ &\quad \left. + E_2\left(I, J, K - \frac{1}{2}\right) \right]^{n}. \end{aligned} \tag{9}$$

Again, the index permutations are employed to obtain H^2 and H^3.

It is worthwhile mentioning here that the use of the contravariant and covariant components of the $\vec{E}$ and $\vec{H}$ fields in the finite difference forms is what distinguishes our formulation from that of Holland [2]. An important advantage of the present approach is that (8) and (9) have exactly the same form as the conventional cartesian FDTD algorithm.

As a final step in our formulation, we need to convert the contravariant components of $\vec{E}$ into its covariant components, in order to calculate the contravariant components of $\vec{H}$, and vice versa. This can be accomplished by noting that the original bases A_i are related to the dual bases through the metric tensor g_{ij} [4], according to

$$A_i = \sum_j g_{ij} A^j; \quad g_{ij} = A_i \cdot A_j. \tag{10}$$

Thus, the covariant components of $\vec{H}$, for instance, H_i, can be obtained from the contravariant components of $\vec{H}$ as follows:

$$H_i = \sum_j g_{ij} H^j \tag{11}$$

By averaging the neighboring values, we have the finite difference approximation of (11). For example, the covariant component H_1 can be written as

$$\begin{aligned} H_1(I, J, K) &= g_{11} H^1(I, J, K) + \frac{g_{12}}{4}\left[H^2\left(I + \frac{1}{2}, J - \frac{1}{2}, K\right)\right. \\ &\quad + H^2\left(I - \frac{1}{2}, J - \frac{1}{2}, K\right) \\ &\quad + H^2\left(I + \frac{1}{2}, J + \frac{1}{2}, K\right) \\ &\quad \left. + H^2\left(I - \frac{1}{2}, J + \frac{1}{2}, K\right)\right] \\ &\quad + \frac{g_{13}}{4}\left[H^3\left(I, + \frac{1}{2}, J, K - \frac{1}{2}\right)\right. \\ &\quad + H^3\left(I - \frac{1}{2}, J, K - \frac{1}{2}\right) \\ &\quad + H^3\left(I + \frac{1}{2}, J, K + \frac{1}{2}\right) \\ &\quad \left. + H^3\left(I - \frac{1}{2}, J, K + \frac{1}{2}\right)\right]. \end{aligned} \tag{12}$$

Similar expressions can be obtained for the other covariant components of either $\vec{E}$ or $\vec{H}$ fields.

Equation (12) represents the only additional computation required in the present formulation over and above that in the cartesian form of the FDTD algorithm. Therefore, the number of operations in the nonorthogonal FDTD is roughly three times that of cartesian FDTD algorithm, provided that the same number of mesh points are used. Of course, as pointed out earlier, the primary motivation for using the nonorthogonal algorithm is to reduce the number of mesh points substantially as compared to the uniform cartesian mesh.

III. Stability Analysis

For a numerical algorithm based upon the finite difference approximation to converge, the necessary and sufficient condition is that the scheme must both be consistent as well as stable [5]. The consistency condition, which is reflected in the Taylor expansions of replacing the differential operators with difference operators, requires that the local truncation error approaches zero as the cell size $h \to 0$. Consequently, to assure the convergence of the numerical procedure presented in this paper, we only need to prove that it is stable for the chosen time step. Therefore, in this section, we derive the stability conditions for the nonorthogonal FDTD algorithm in two and three dimensions. To derive the stability conditions, we appeal to the causality consideration for the two-dimensional case, and employ a more rigorous mathematical treatment for the three-dimensional case.

A. Two-Dimensional Case

Fig. 2 shows a typical non-Cartesian cell in two dimensions, where h represents the closest distance between two lattice planes in this non-Cartesian lattice. Since energy can not propagate faster than the speed of light, the law of causality requires that the time step Δt, in the non-orthogonal FDTD algorithm, be less than the shortest travel time h/c for the wave between the lattice planes. However, from Fig. 2, we see that

$$h = \frac{\sqrt{g}}{\sqrt{(\boldsymbol{A}_1 - \boldsymbol{A}_2) \cdot (\boldsymbol{A}_1 - \boldsymbol{A}_2)}} = \frac{\sqrt{g}}{\sqrt{g_{11} + g_{22} - 2g_{12}}}. \tag{13}$$

In two dimensions, $\sqrt{g}$ reduces to the area of the cell. Consequently, the necessary stability criterion is obtained as

$$\Delta t \le \frac{1}{c}\left(\frac{\sqrt{g}}{\sqrt{g_{11} + g_{22} - 2g_{12}}}\right). \tag{14}$$

This condition was first provided by Fusco [3]. Unfortunately, however, there appears to be a typographical error in his formula in [3].

In the numerical implementation, the r.h.s. of (14) is evaluated at every grid point, the smallest value is then used as the upper bound for choosing the time step in the nonorthogonal FDTD algorithm.

B. Three-Dimensional Case

To derive the stability condition for three-dimensional nonorthogonal FDTD algorithm, we start from the vector wave equation:

$$\nabla \times \nabla \times \vec{E} = \frac{-1}{c^2}\frac{\partial^2 \vec{E}}{\partial t^2}. \tag{15}$$

As is well known [6], an arbitrary wave can be expanded in terms of a spectrum of plane waves which can also be viewed as the eigenmodes of the wave equation. Next, we argue that a time domain procedure must be stable for an arbitrary plane wave. Consequently, we let

$$\begin{aligned} \vec{E}(u^1, u^2, u^3; t) &= \vec{\mathcal{E}}(t) \exp(-j\vec{k} \cdot \vec{r}) \\ &= \vec{\mathcal{E}}(t) \exp(-j[k_1 u^1 + k_2 u^2 + k_3 u^3]) \end{aligned} \tag{16}$$

where

$$k_i = \vec{k} \cdot \boldsymbol{A}_i \tag{17}$$

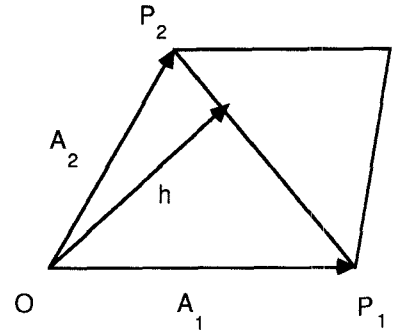

Fig. 2. Typical two-dimensional non-Cartesian cell.

In a general nonorthogonal coordinate system, the operator ∇ becomes

$$\nabla = A^1 \frac{\partial}{\partial u^1} + A^2 \frac{\partial}{\partial u^2} + A^3 \frac{\partial}{\partial u^3} \tag{18}$$

Substituting (16) into (18), performing the central differencing for each of the spatial derivative and making use of $\Delta u^i = 1$, the ∇ operator can be replaced symbolically by

$$\nabla = -2j \sum_i \left(A^i \sin \left[\frac{\Delta (k_i u^i)}{2} \right] \right) \tag{19}$$

Furthermore, any plane wave with a representation given in (16) satisfies the divergence-free condition. Therefore, (15) reduces to

$$(\nabla \cdot \nabla) \vec{E} = \frac{1}{c^2} \frac{\partial^2 \vec{E}}{\partial t^2} \tag{20}$$

Defining a solution growth factor $\lambda = \vec{E}^{n+1}/\vec{E}^n$, and substituting (19) into (20), we obtain

$$-4 \left\{ \sum_l \left(A^l \sin \left[\frac{\Delta (k_l u^l)}{2} \right] \right) \cdot \sum_m \left(A^m \sin \left[\frac{\Delta (k_m u^m)}{2} \right] \right) \right\} \vec{E} = \frac{1}{c^2} \frac{\lambda^2 - 2\lambda + 1}{\lambda \Delta t^2} \vec{E}. \tag{21}$$

Solving (21) for λ we get

$$\lambda = (1 - 2s^2 \Delta t^2) \pm 2s \Delta t \sqrt{s^2 \Delta t^2 - 1}$$

where

$$s^2 = c^2 \sum_{\substack{l=1 \\ m=1}}^{3} \left(A^l \cdot A^m \sin \frac{\Delta (k_l u^l)}{2} \sin \frac{\Delta (k_m u^m)}{2} \right). \tag{22}$$

The numerical scheme would be stable if the growth factor $|\lambda| \leq 1$. From (22) we see that this condition is satisfied if and only if

$$s^2 \Delta t^2 \leq 1. \tag{23}$$

Furthermore, as pointed out earlier, the above condition must hold for an arbitrary plane wave. This can be assured by noting that for all possible waves, we have

$$s^2 \leq c^2 \sum_{\substack{l=1 \\ m=1}}^{3} (g^{lm})$$

where

$$g_{lm} = A^l \cdot A^m. \tag{24}$$

Hence, to satisfy the stability condition (23) for all the spatial modes in the lattice, we set

$$\Delta t \leq \frac{1}{c \sqrt{\sum_{\substack{l=1 \\ m=1}}^{3} g_{lm}}}. \tag{25}$$

In an attempt to extend the stability condition to a more general form, and hopefully provide more insights, we will show that the square-root term in (25) is related to the norm of the ∇ operator in the nonorthogonal FDTD algorithm. Typically the norm of an operator, for instance ∇, is defined as

$$\| \nabla \| = \sup_W \frac{\| \nabla W \|}{\| W \|} \tag{26}$$

where $\| \cdot \|$ is the usual L_2 norm, W is any admissible function in the solution process, and sup represents the upper-bound. In particular, since plane waves form a complete set of basis functions, therefore W in (26) can be limited to only plane waves, i.e.,

$$\| \nabla \| = \sup_{k_1 k_2 k_3} \| \nabla W \|,$$

$$W = \exp(-j[k_1 u^1 + k_2 u^2 + k_3 u^3]) \tag{27}$$

Substituting (19) into (27), the result is

$$\| \nabla \| = 2 \sup_{k_1 k_2 k_3} \cdot \sqrt{\sum_{\substack{l=1 \\ m=1}}^{3} A^l \cdot A^m \sin \left(\frac{\Delta [k_l u^l]}{2} \right) \sin \left(\frac{\Delta [k_m u^m]}{2} \right)} = 2 \sqrt{\sum_{\substack{l=1 \\ m=1}}^{3} g^{lm}}. \tag{28}$$

Using (28), we rewrite (25) as

$$\Delta t \leq \frac{2}{c \| \nabla \|}. \tag{29}$$

Note that (29) is based on the assumption that central-differencing is employed for both time and space derivatives. Finally, we demonstrate that (29) reduces to the familiar forms in a Cartesian system:

Two-Dimensional Case:

$$\| \nabla \| = \sup_E \frac{\| \nabla E \|}{\| E \|} = 2 \sqrt{\frac{1}{(\Delta x)^2} + \frac{1}{(\Delta y)^2}} \pi \rightarrow \Delta t \leq \frac{1}{c \sqrt{\frac{1}{(\Delta x)^2} + \frac{1}{(\Delta y)^2}}}$$

Three-Dimensional Case:

$$\|\nabla\| = \sup_{E} \frac{\|\nabla E\|}{\|E\|}$$

$$= 2\sqrt{\frac{1}{(\Delta x)^2} + \frac{1}{(\Delta y)^2} + \frac{1}{(\Delta z)^2}} \to \Delta t$$

$$\leq \frac{1}{c\sqrt{\frac{1}{(\Delta x)^2} + \frac{1}{(\Delta y)^2} + \frac{1}{(\Delta z)^2}}}. \quad (30)$$

IV. Numerical Results

Several numerical examples are presented in this section to demonstrate the validity of the non-orthogonal FDTD algorithm. The problems considered are: 1) *H*-plane waveguide junction; 2) circular waveguide with a circular iris; 3) circular waveguide with a rectangular iris; and, 4) 45° microstrip bend discontinuity. The numerical results of Section IV-A–D are for the steady-state responses which have been derived by using a sinusoidal signal as the excitation. However, in Section IV-D the reflection coefficient of the discontinuity is obtained from time domain results of a Gaussian pulse excitation.

A. H-Plane Waveguide Junction

Figure 3 shows the cross-section of an *H*-plane waveguide junction. The height of the junction is uniform and, therefore, this is essentially a two-dimensional problem. By using the three-dimensional non-orthogonal FDTD algorithm to model it, we can compare our results with an existing two-dimensional FEM approach [8]. Also, shown in Fig. 3 is a plane-cut of the nonorthogonal mesh that is employed for the current analysis. Note that this problem is solved without using any absorbing boundary conditions; consequently, the problem domain has to be truncated very far away from the discontinuity region as can be seen from the figure. The computed steady state field distribution along the length of the discontinuity region is plotted in Fig. 4, where the unit of the distance is arbitrary. In Fig. 4, we also show the comparison of the current results with the ones obtained from the frequency domain finite-element analysis [8]. Very close agreement between the two results is observed.

B. Circular Waveguide with a Circular Iris

Fig. 5 shows a circular waveguide with a circular iris. The waveguide is filled with an isotropic dielectric material of dielectric constant 9.7, except the thin iris region which is filled with air. This problem has been analyzed using two techniques, viz., the mode matching method and the nonorthogonal FDTD approach. In the nonorthogonal FDTD approach, the cross-section of the mesh that is used is shown in Fig. 6. Since the problem is symmetric, only a quarter of the geometry is modeled. The three-dimensional mesh is generated by extruding the two-dimensional mesh (see Fig. 6) in the third dimension. By using the first-order ABC [9], we are able to bring the artificial truncation boundaries to distances as close as 1λ away from the iris for a frequency of 6 GHz. The computed reflection and transmission coefficients derived from these two approaches are shown in Figs. 7 and 8. Good agreement between the two results confirm the validity of the nonorthogonal FDTD approach.

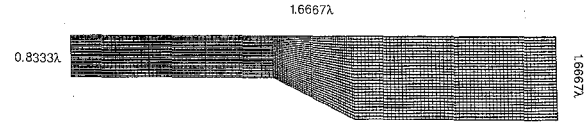

Fig. 3. Nonorthogonal mesh for an *H*-plane waveguide junction.

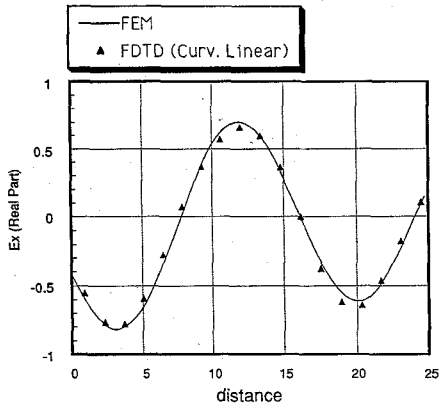

Fig. 4. Field distribution along the taper region.

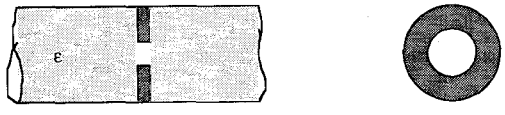

Fig. 5. Circular waveguide with a circular iris.

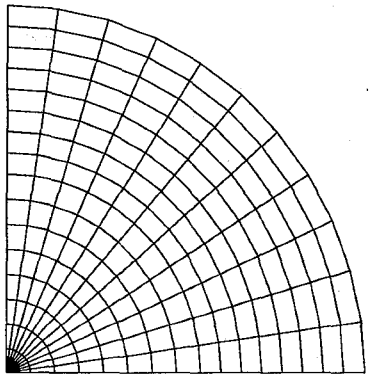

Fig. 6. Cross-section of the nonorthogonal mesh for the iris discontinuity problem shown in Fig. 5.

C. Circular Waveguide with a Rectangular Iris

The mesh used to investigate a circular dielectric-loaded waveguide with a thin rectangular iris is shown in Fig. 9.

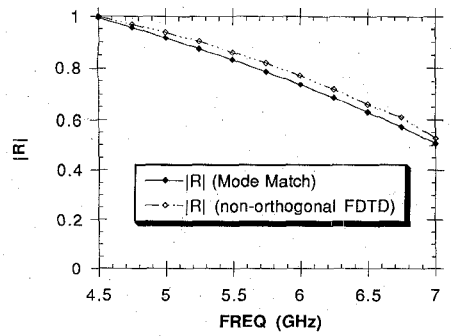

Fig. 7. Comparison of the numerical results for the reflection coefficient for the circular iris dioscontinuity computed by using the mode matching and the nonorthogonal FDTD algorithm.

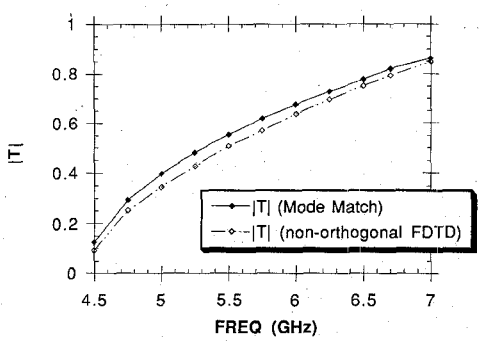

Fig. 8. Comparison of the numerical results for the transmission coefficient for the circular iris discontinuity problem.

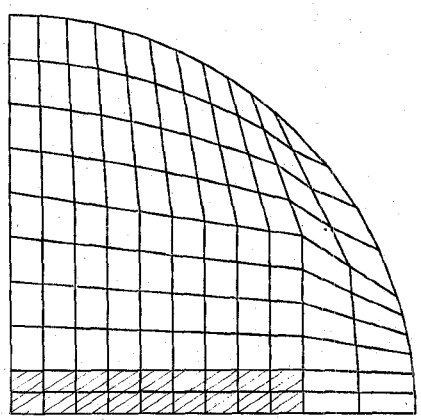

Fig. 9. Cross-sectional mesh for a circular waveguide with a rectangular iris.

The dielectric constant of the dielectric is 9.7, the radius of the waveguide is 6.35 mm, and the dimensions of the aperature is 1.3716 mm × 9.1948 mm. Again, this two-dimensional mesh is extrapolated into the third dimension to generate the required three-dimensional computational grid. The use of ABC again allows us to bring the truncation boundaries to 1λ away from the iris at 6 GHz. The computed reflection and transmission coefficients are plotted in Figs. 10 and 11, respectively. It has not been possible to compare these results with others owing to the unavailability of published results for this geometry in the literature.

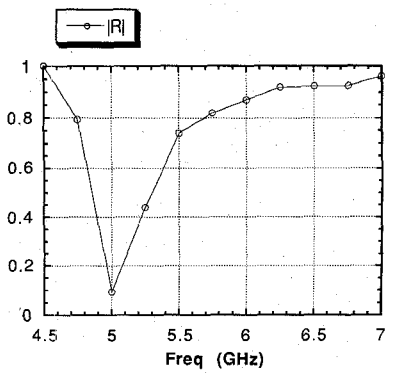

Fig. 10. Computed reflection coefficient for the rectangular iris problem using the nonorthogonal FDTD algorithm.

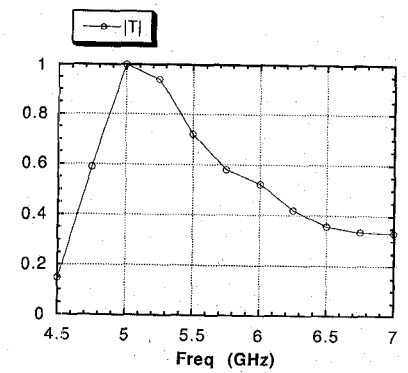

Fig. 11. Computed transmission coefficient for the rectangular iris discontinuity.

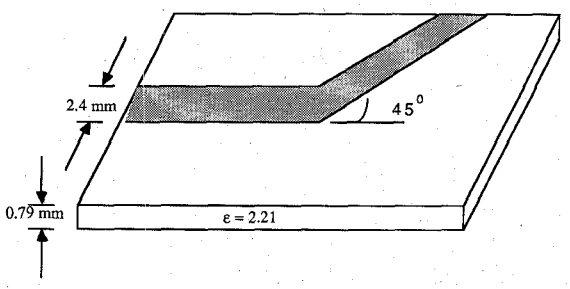

Fig. 12. A 45° microstrip bend discontinuity.

D. 45° Microstrip Bend Discontinuity

Another problem investigated by using the nonorthogonal time domain approach is the 45° microstrip bend shown in Fig. 12, which is conveniently analyzed using the nonorthogonal mesh approach that avoids staircasing. Fig. 13 displays the return loss versus frequency curves obtained by using: 1) the nonorthogonal FDTD approach; 2) the microwave computer-aided design package TOUCHSTONE; 3) a lossless T circuit model for the discontinuity; and 4) HP8510B network analyzer. We note that below 6 GHz, which is believed to be the upper limit for accurate measurements because of the connectors used, the agreement between the nonorthogonal FDTD and the measured results is good.

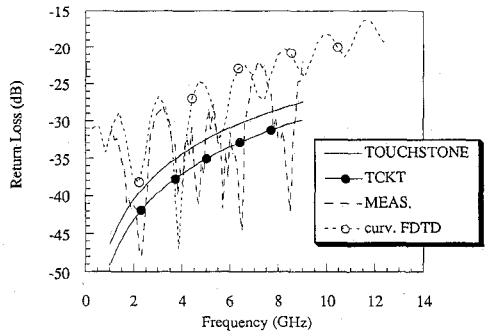

Fig. 13. Numerical results for three models versus experiment for the 45° bend.

V. Conclusion and Discussion

In this paper, we have reformulated the nonorthogonal FDTD algorithm, using the covariant and contravariant components of the electric and magnetic fields as the unknown variables, to result in a more efficient time marching procedure than that presented in [2]. Additionally, we have performed the stability analyses of the nonorthogonal FDTD algorithm in two and three dimensions, and derived an upper bound for the time step that guarantees stable numerical solutions. Finally, the modified nonorthogonal FDTD algorithm has been applied to study several waveguide discontinuities, viz., an *H*-plane waveguide junction, a circular waveguide with a circular iris, a circular waveguide with a rectangular iris, and a 45° microstrip bend. The computed results compared favorably with previously available techniques and, therefore, validated the present approach.

References

[1] K. S. Yee, "Numerical solution of initial boundary value problems involving Maxwell's equations in isotropic media," *IEEE Trans. Antennas Propagat.*, vol. AP-14, pp. 302–307, May 1966.

[2] R. Holland, "Finite-difference solution of Maxwell's equations in generalized nonorthogonal coordinates," *IEEE Trans. Nucl. Sci.*, vol. NS-30, no. 6, Dec. 1983.

[3] M. Fusco, "FDTD algorithm in curvilinear coordinates," *IEEE Trans. Antennas Propagat.* vol. 38, pp. 76–88, Jan. 1990.

[4] J. A. Stratton, *Electromagnetic Theory*. New York: McGraw-Hill, 1941.

[5] G. Strang and G. J. Fix, *An Analysis of the Finite Element Method*. Englewood Cliffs, NJ: Prentice Hall, 1973.

[6] W. C. Chew, *Waves and Fields in Inhomogeneous Media*. New York: Van Nostrand Reinhold, 1990.

[7] E. Kreyszig, Introductory Functional Analysis with Applications. New York: Wiley, 1978.

[8] Z. J. Cendes and J. F. Lee, "The transfinite element method for modeling MMIC devices," *IEEE Trans. Microwave Theory Tech.*, vol. 36, pp. 1639–1649, Dec. 1988.

[9] J. F. Lee and R. Mittra, "Analysis of microwave ferrite devices by using finite element method," *J. Appl. Phys.*, vol. 69, pp. 5032–5034, Apr. 1991.

Jin-Fa Lee was born in Taipei, Taiwan, in 1960. He received the B.S. degree from National Taiwan University, in 1982 and the M.S. and Ph.D. degrees from Carnegie Mellon University in 1986 and 1989, respectively, all in electrical engineering.

From 1988 to 1990, he was with ANSOFT Corp., where he developed several CAD/CAE finite element programs for modeling three-dimensional microwave and millimeter-wave circuits. From 1990 to 1991, he was Post-Doctoral Fellow at the Electromagnetic Communication Laboratory, University of Illinois at Urbana-Champaign. Currently, he is an Assistant Professor at Department of Electrical Engineering, Worcester Polytechnic Institute. Dr. Lee's current research interests are analyses of numerical methods, couplings of active and passive components in the high-speed electronic circuits, solution of the moving boundary problem and its application to semiconductor process modelings, and EM field propagation in linear and/or non-linear medium.

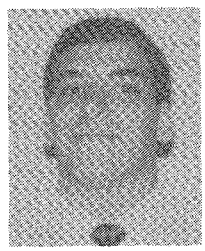

Robert Palandech was born in Chicago Heights, IL, on January 12, 1967. He received the B.S. degree in electrical engineering with High Honors from the University of Illinois at Urbana-Champaign in 1989. He continued his studies at the University of Illinois and was a University of Illinois Fellow for the 1989–90 academic year. He was a Research Assistant with the Electromagnetic Communication Laboratory from 1990 to 1991, investigating time domain Maxwell solvers, and received the M.S.E.E. degree in May 1991.

He has been with Motorola, Inc. Corporate Research Laboratories in Schaumburg, IL, since June 1991. His technical interests include electromagnetic modeling and hardware design for land mobile communications product.

M. Palandech is a member of Eta Kappa Nu and Tau Beta Pi.

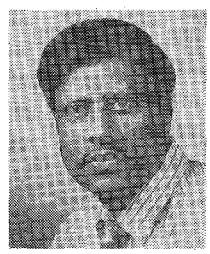

Raj Mittra (S'54–M'57–SM'69–F'71) is Director of the Electromagnetic Communication Laboratory of the Electrical and Computer Engineering Department and Research Professor of the Coordinated Science Laboratory at the University of Illinois. He is a former president of AP-S, and he has served as the editor of the IEEE Transactions on Antennas and Propagation. He is president of RM Associates, a consulting organization providing services to several industrial and governmental organizations.

Dr. Mittra's professional interests include the areas of analytical and computer-aided electromagnetics, high-speed digital circuits, radar scattering, satellite antennas, microwave and millimeter-wave integrated circuits, frequency selective surfaces, EMP and EMC analysis, and remote sensing.